Applied Catalysis B: Environment and Energy 344 (2024) 123627

Contents lists available at ScienceDirect

Applied Catalysis B: Environment and Energy

journal homepage: www.elsevier.com/locate/apcatb

Precisely designed cobalt single atom on ZrO_2 support for chemical CO_2 fixation

Neha Choudhary [a], Shan Jiang [b], Hien Pham [c], Gotluru Kedarnath [d], Abhaya Datye [c], Jeffrey T. Miller [b], Avesh Kumar Tyagi [d], Mobin M. Shaikh [a,e,*]

[a] Department of Chemistry, Indian Institute of Technology Indore, Simrol Khandwa Road, 433552, India
[b] Davidson School of Chemical Engineering, Purdue University, West Lafayette, IN 47907, United States
[c] Department of Chemical Biological Engineering and Center for Micro-Engineered Materials, University of New Mexico, Albuquerque, NM 87131, United States
[d] Chemistry Division, Bhabha Atomic Research Centre, Mumbai 400085, India and Homi Bhabha National Institute, Anushaktinagar, Mumbai 400094, India
[e] Center for Advanced Electronics, Indian Institute of Technology Indore, Simrol Khandwa Road, 433552, India

A R T I C L E I N F O

Keywords:
Single atom catalyst
CO_2 fixation
Solvent-free
Recyclable catalyst
Co doped ZrO_2 catalyst

A B S T R A C T

The presence of single atoms as active sites on a metal oxide support can dramatically enhance catalytic activity. Here, we demonstrate that Cobalt doped ZrO_2 constitutes a single atom catalyst where each Co^{+2} ion act as active for CO_2 fixation. The synthesized Co/ZrO_2 catalyst was characterized by EXAFS and STEM to confirm the presence of isolated Co^{+2} on the ZrO_2 support. The STEM-EDS data showed a uniform distribution of Co over the surface of the ZrO_2 support. The catalytic results reveal that Co active sites on ZrO_2 enhance catalytic performance and provide ~100% conversion into carbonate products in the presence of trace amounts of tetrabutylammonium bromide (TBAB). When undoped ZrO_2 and Co_3O_4 impregnated ZrO_2 catalyst was utilized for comparison, less than 50% conversion of epoxides was obtained. The single atom catalyst (SAC) showed a broad substrate scope, solvent-free reaction and higher catalytic activity and selectivity.

1. Introduction

Heterogeneous catalysis has entered a new phase with the development of single-atom catalysts (SACs), in which the isolated active metal atoms are anchored to supports [1–4]. In SACs, every surface atomic site is accessible which delivers superior catalytic performance and the highest atom utilization efficiency [5,6]. SACs act as a bridge between homogeneous and heterogeneous catalysts as they posesses properties of both type of materials i.e. recyclability and easy recoverability, thermal stability and better exposure of active sites. For industrial applications, recyclability, cost-effectiveness and catalytic performance are the key requirements. In comparison to nanoparticle catalysts, SACs have demonstrated impressive enhancements in catalytic activity in various catalytic processes due to their distinct structural characteristics and fully exposed active sites [7–10]. However, the synthesis and stabilization of SACs is a challenging task due to the high surface energy of the isolated atoms, resulting in agrregation of SACs and decrease in catalytic activity.[11–13] For synthesizing SACs, various stratagies like doping, utilization of defects and spatial confinement have been utilized to stabilize the single atom over different supports [11,14,15]. Moreover, characterization of SACs remains a daunting task since it requires atomic level high resolution in techniques like STEM-HAADF and EELS. The conventional transmission electron mircoscopes are unable to observe single atoms on supported materials owing to their contrast mechanisms [16]. Aberration-corrected HAADF-STEM is extremely sensitive to atomic number of the atoms present in the sample. However, it is still challenging to observe single atoms when the difference in atomic numbers of the isolated atoms and the support is not enough to provide sufficient contrast [17]. Since AC-STEM is a local technique, it is necessary to combine information with techniques that provide an average over the entire sample, like EXAFS, and XANES while also yielding information on oxidation states and bond distances for nearest neighbors for the supported single atoms [18].

Recently, SACs were explored for electrocatalytic, thermal and photocatalytic CO_2 hydrogenation and valorization reactions due to their enhanced catalytic performance [4,19–23]. SACs provide more exposure to active sites and result in product selectivity and enhancement in catalytic activity. An ideal catalyst would have a low energy barrier, selectivity towards the desired product, easy synthesis, recoverability and cost-effectiveness.[24] SACs of non-noble metals have all

* Corresponding author at: Department of Chemistry, Indian Institute of Technology Indore, Simrol Khandwa Road, 433552, India.
E-mail address: xray@iiti.ac.in (M.M. Shaikh).

https://doi.org/10.1016/j.apcatb.2023.123627
Received 29 August 2023; Received in revised form 4 December 2023; Accepted 9 December 2023
Available online 18 December 2023
0926-3373/

these advantanges, which can reduce the process cost while increasing the catalytic performance without compromising selectivity towards desired products.[25,26] Hence, SACs of non-noble metals are the best choice for CO_2 conversion into value-added products. Carbon dioxide is the major greenhouse gas which leads to climate change and global warming. Thus, the conversion of CO_2 into value-added products can help achieve sustainablity and carbon neutrality. Previous efforts to utilize or capture CO_2 have explored the production of value added products like cyclic caronates, urea, methanol, etc. However, owing to its high thermodynamic stability, the conversion of CO_2 requires high pressure and temperture. Also, achieving selectivity towards one product is a desirable goal for CO_2 conversion, otherwise in the case of CO_2 hydrogenation we can produce methanol, methane, formate, formic acid, etc. [27,28].

CO_2 fixation and reaction with epoxides to yield cyclic carbonates has potential to produce many commercial products since there are few undesirable side products.[29] The cycloaddition of CO_2 with epoxides is useful for the synthesis of plastics, cosmetics and adhesives [30,31]. These are useful as intermiadiates for various synthetic processes and also as electrolytes in lithium-ion batteries.Cyclic carbonates have also been utilized to synthesize commercially significant compounds including polycarbonates, polyurethanes, and dialkyl carbonates etc. [32] Traditionally cyclic carbonates were synthesized using highly toxic phosgene, which is banned in many countries. Hence, the synthesis of cyclic carbonates from cycloaddition reaction of epoxides and carbon dioxide is a promising pathway.

Recently, various metal organic frameworks (MOFs) of Cu [33], Pd@Eu [34], Ca based [35], Yttrium [36], thulium [37], Zn [38,39] and Ln based coordinated polymers[40] have been explored for the CO_2 fixation of expoxides with tetrabuthylammonium halogen containing reagent (TBAX) at 70–100℃ for 4–24 h and under solvent-free reaction conditions. Furthermore, $CuCo_2O_4$ spinel[30], phenolated lignin NPs [41], ligated Ti coated Bi-oxo cores[42], PABA@ α-Fe_2O_3[43] and N,S co-doped bifunctional carbon catalyst[44] were also explored using TBAX at room temperature to 105℃ for 3–24 h. In all cases moderate to good yield was obtained but the reaction time and TBAX amount required was reatively high even at high reaction temperature. However, ionic liquid-based and halide-free reactions were also reported at 60–90℃ and 12–48 h reaction times with poor substrate scopes.[29,45, 46] Several SACs were recently reported for cycloaddition of CO_2 into epoxides; [47–50] however, these all showed narrow substrate scope or required solvents like DCM and DMF.

Herein, we synthesized a Co/ZrO_2 SAC via a facile coprecicipitation method and characterized extensively it with EXAFS, STEM, HAADF and XANES techniques to confirm the presence of single atoms and utilized it for catalytic conversion of epoxides into cyclic carbonates. The single atom catalyst showed superior catalytic activity compared to undoped ZrO_2 and Co_3O_4/ZrO_2 catalyst. The Co/ZrO_2 SAC showed 100% conversion into cyclic carbonate product with minimal amount of TBAB (0.06 mmol) in solvent-free conditions which makes it cost-effective, greener, and environmentally benign[43,51], whereas undoped ZrO_2 and Co_3O_4/ZrO_2 catalyst showed less than 50% conversion, confirming that the single atom catalyst provides more active sites. The catalyst showed broad substrate scope with excellent yield in all the cases with recyclability of up to six cycles.

2. Experimental section

2.1. Materials

Cobalt nitrate hexahydrate ($Co(NO_{3)2}$. 6 H_2O) ≥ 99% pure and zirconyl nitrate hydrate ($ZrO(NO_3)_2$. xH_2O) anhydrous ≥ 99.99% pure were purchased from SRL chemicals, India. Ammonia solution was purchased from Merck, India. Reagents and epoxides compounds ≥ 98–100% pure were purchased from Sigma-Aldrich and TCI, India. All solvents were used as received.

2.2. Catalyst synthesis

2.2.1. Synthesis of Co doped ZrO_2

For synthesizing Co doped ZrO_2, firstly Cobalt nitrate hexahydrate and Zirconyl nitrates hydrates (1:9 molar ratio) were taken in round bottom flask in 50 mL water and stirred the mixture for 20 min. To maintain the pH ∼ 9, ammonia solution was added dropwise with continuous stirring. During this addition of ammonia solution colour changes from light pink to bluish pink colour. After stirring the mixture for next 1 h, the solution was centrifuged and washed several times with water till pH∼7 and then dried overnight at 100 ℃. Thereafter, the solid precipitate was calcined at 500 ℃ for 3 h with ramping temperature 2 ℃/min. The synthesized catalyst is named as Co/ZrO_2 single atom catalyst.

2.2.2. Synthesis of undoped ZrO_2

The undoped ZrO_2 catalyst was synthesized using zirconyl nitrate with above mentioned method without using cobalt nitrate.

2.2.3. Synthesis of Co_3O_4 supported on ZrO_2

For synthesizing cobalt impregnated ZrO_2 catalyst, as synthesized ZrO_2 was initially taken in round bottom flask and stirred it into water for 20 min at room temperature. In another beaker, $Co(NO_{3)2}$. 6 H_2O was dissolved in 10 mL water and added dropwise to the above dispersed solution of ZrO_2 and allowed to stir the mixture for another 1 h. After 1 h, the solution was evaporated under reduced pressure and the precipitates were dried overnight at 100 ℃ and then calcined at 500 ℃ for 3 h with ramping temperature 2 ℃/min. The synthesized catalyst is named as Co_3O_4/ZrO_2 catalyst.

2.3. General catalytic reaction

In a general CO_2 fixation reaction, epoxide substrates (10 mmol) were added with catalyst (15 mg), TBAB (0.06 mmol) in stainless steel containing Teflon reaction vessel pressure reactor attached with thermocouple at magnetic stirring bar. After closing the reactor, the reaction vessel was flushed three times with CO_2 to replace the existing air and then pressurized with 2 bar pressure and keep it for stirring at 80 ℃ for required reaction time. After completion of reaction, the reactor was cooled down to room temperature and pressure was released. The reaction mixture was centrifuged for catalyst separation and in the obtained reaction mixture, 0.1 mmol (14 μL) mesitylene as internal standard was added and diluted with methanol and given for GC-MS analysis to analyze the conversion and selectivity. For NMR analysis, the reaction mixture was diluted with ethyl acetate and dried under rotavapor and then given for analysis to confirm the product formation. Additionally, for recycle study, the centrifuged catalyst was then washed, dried overnight at room temperature, and used for next cycle.

2.4. Physicochemical characterization

Powder x-ray diffraction (PXRD) of the nanoparticle performed using Cu Kα radiation (1.54 Å) using the Rigaku Smart Lab X-ray diffractometer. Thermogravimetric analysis was performed using METTLER TOLEDO (TGA/DSC 1) to evaluate the thermal stability of SAC. The Brunauer–Emmett–Teller (BET) surface area was determined using N_2 and CO_2 adsorption-desorption measurements. The morphology was analysed by using Supra55 Zeiss Field Emission Scanning Electron Microscopy (Supra55 Zeiss FE-SEM) and FEI Tecnai G2 F30 Field Emission Gun-Transmission Electron Microscopy (HR-TEM, operable at 300 kV). The X-ray Photoelectron Spectroscopy (XPS) analysis of fresh catalysts was recorded using Scient Omicron Multiprobe XPS spectrometer.

Samples were dispersed in ethanol and mounted on holey carbon grids for examination in a JEOL NEOARM 200CF transmission electron microscope equipped with spherical aberration correction to allow atomic resolution imaging, and an Oxford Aztec Energy Dispersive

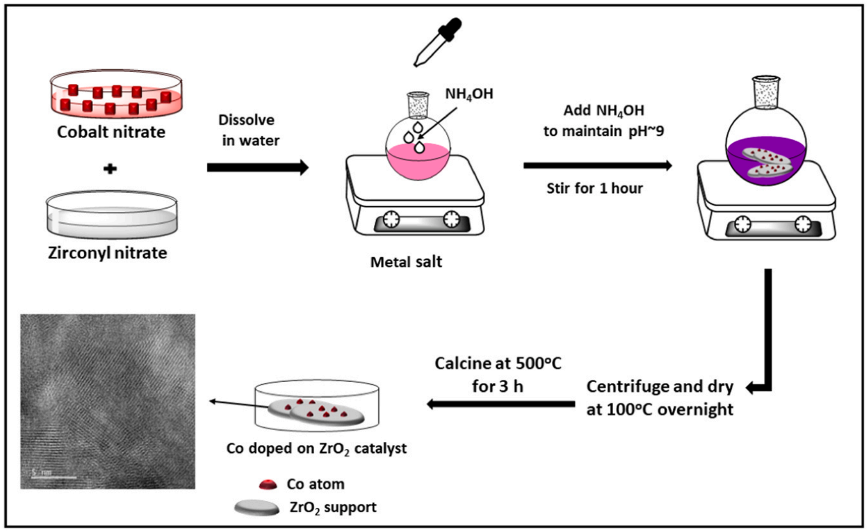

Scheme 1. Schematic representation of the synthesis of Co/ZrO_2 catalyst.

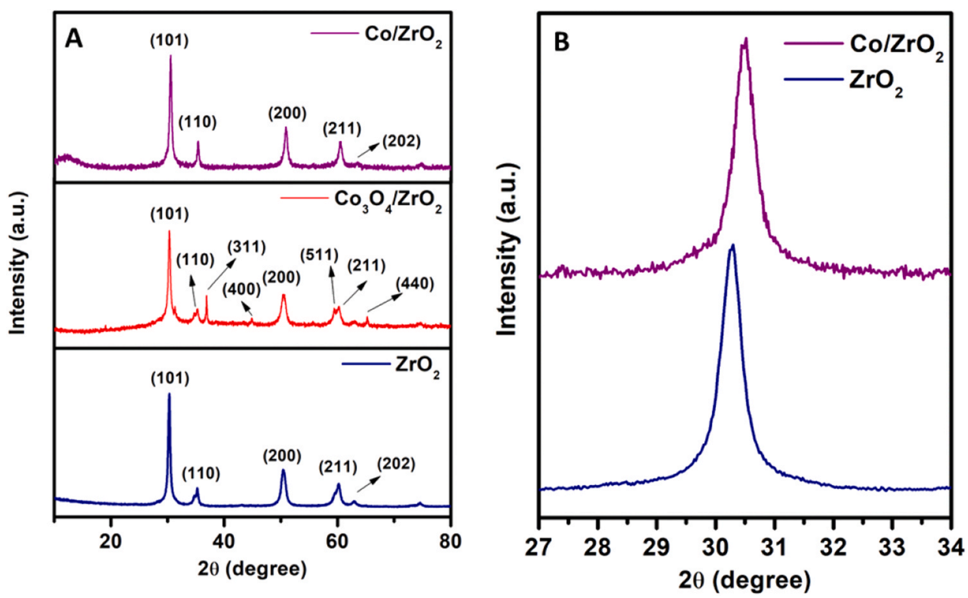

Fig. 1. **(A)** PXRD of Co/ZrO_2 single atom catalyst, Co_3O_4 supported on ZrO_2 and undoped ZrO_2 and (**B**) shifting of (101) plane of ZrO_2 with doping of cobalt.

System (EDS) for elemental analysis. The microscope is equipped with two large area JEOL EDS detectors for higher throughput in acquisition of x-ray fluorescence signals. Images were recorded in annular dark field (ADF) mode and in annular bright field (ABF) mode.

XAS experiments were performed at 5BM-D beamline of DND-CAT at beamline 5 BM-D (DND-CAT) of the Advanced Photon Source (APS) of Argonne National Laboratory, at Co K (7709 eV) edge. Co/ZrO2 and Co_3O4/ZrO_2 samples were ground to a fine powder by using a pestle and mortar, then evenly spread on long Scotch tape (3 M Corp) to form a uniform sample layer. The tape was folded to create a uniform surface to produce adequate absorption. The sample was mounted vertically on a sample holder with its surface normal bisecting the 90 angles between the X-ray incidence and photon detecting directions. A double crystal Si (111) monochromator was used for energy selection. Both Co K-edge XANES and EXAFS were measured under fluorescence mode by a Vortex ME4 detector. Metal Co foil transmission spectrum for energy calibration was collected along with each sample. XAS data were processed using WinXAS software [52]. Simulated phase and amplitude functions for Co-O scattering were extracted using Feff6.[53] The extracted *chi* was k^2-weighted and Fourier transformed over a k range of 2.5 to 10 Å^{-1} for the samples. The S_0^2 value was determined by fitting the Co foil reference compound. Fitting was performed in q-space to determine the Debye-Waller factor, $\Delta\sigma^2$. The final EXAFS fits were conducted in R-space.

The catalyst leaching was performed using ICP-Atomic Emission Spectroscopy (Model: ARCOS, Simultaneous ICP Spectrometer). Identification of the products of catalytic reactions carried out using Shimadzu GC-MS, QP2010 mass spectrometer with with a 30 m long Rxi-5Sil MS separation column with a 0.25 mm diameter and 0.25 μM thickness. The formation of substituted products was confirmed by ^1H and ^{13}C NMR analysis using NMR Spectrometer, Model AVANCE NEO Ascend 500 Bruker BioSpin International AG.

3. Results and discussion

3.1. Characterization of catalyst

The single-atom catalyst Co/ZrO_2 was synthesized via

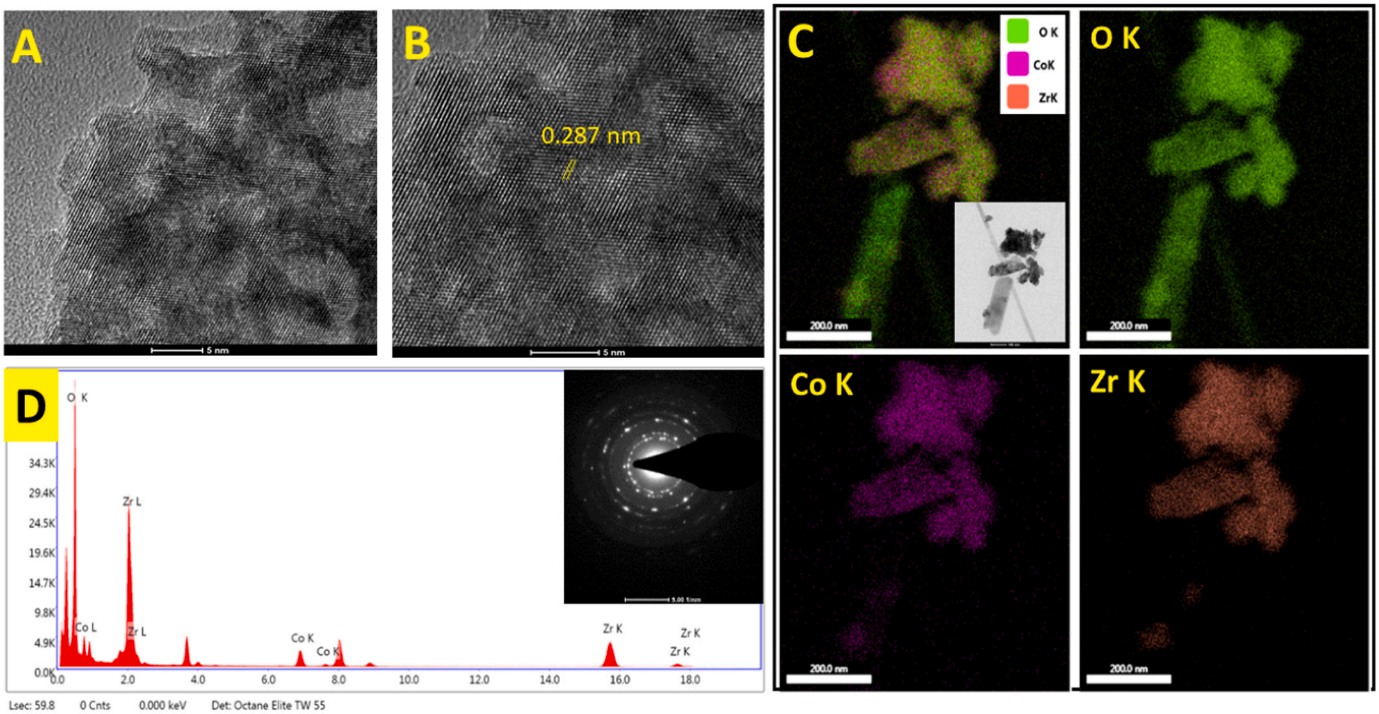

Fig. 2. HR-TEM images of single atom Co/ZrO_2 catalyst at **(A-B)** 5 nm, **(C)** Elemental mapping and **(D)** EDS spectra (inset selected area electron diffraction (SAED) pattern at 5 1/nm).

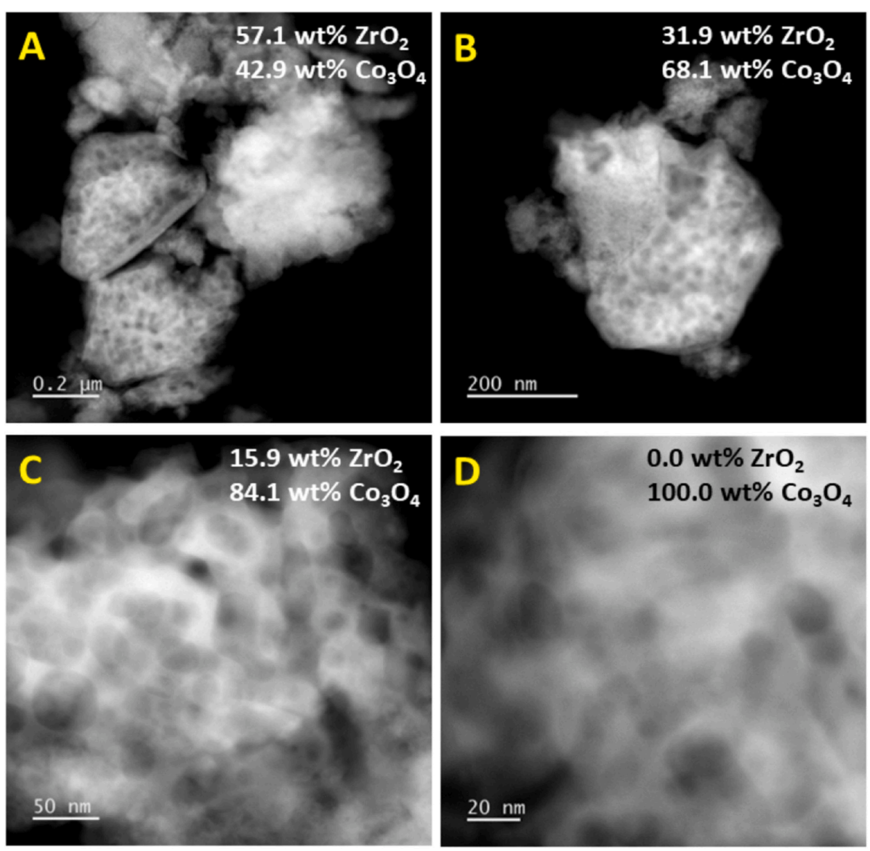

Fig. 3. (A-B) STEM images of impregnated Co_3O_4/ZrO_2 catalyst at different magnifications as indicated by the scale bars of **(A-B)** 200 nm, **(C)** 50 nm, and **(D)** 20 nm with elemental analysis of each field of view listed on the image.

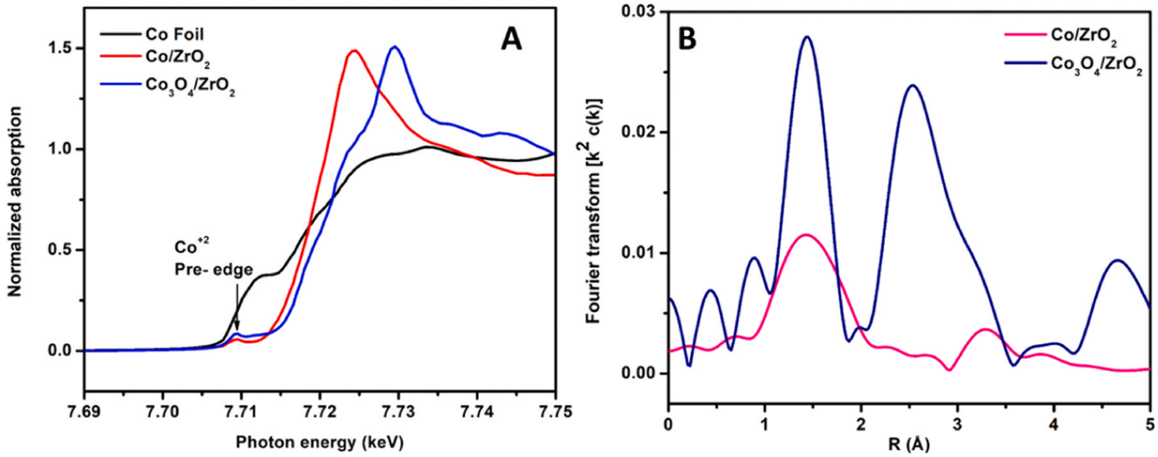

Fig. 4. (A) Co K-edge XANES spectrum of Co/ZrO_2 single atom catalyst (red), Co_3O_4/ZrO_2 impregnated catalyst (blue) along with Co foil (black) as references and **(B)** Fourier transform of Co K-edge EXAFS spectra of Co/ZrO_2 single atom catalyst where k^2: $\Delta k = 2.55$ to 10.0 $Å^{-1}$ and Co_3O_4/ZrO_2 catalyst where k^2: $\Delta k = 2.7$ to 10.2 $Å^{-1}$ in R- space**.**

Table 1
Co K-edge first shell EXAFS fitting results for Co/ZrO_2, Co_3O_4/ZrO_2, Co_3O_4 and reference Co foil where (k^2: $\Delta k = 2.55$ to 10.0 $Å^{-1}$ for Co/ZrO_2, k^2: $\Delta k = 2.7$ – 12.0 $Å^{-1}$ for Co_3O_4/ZrO_2 and $\Delta R = 1.0$ – 3.4 Å) and $^*S_o = 0.80$.

Sample	XANES Pre-Edge Energy (eV)	Edge Energy (eV)	Scatter	CN	R (Å)	ΔE_o (eV)	σ^2
Co foil*	-	7709.0	Co-Co	12.0	2.49	5.7	0.0065
Co_3O_4	7709.3	7717.6	Co-O	5.0	1.92	-0.7	0.004
			Co-O-Co	4.4	2.85	-4.8	0.004
			Co-O-Co	5.5	3.35	-6.0	0.004
Co_3O_4/ ZrO_2	7709.3	7717.6	Co-O	4.8	1.92	0.6	0.005
			Co-O-Co	4.4	2.85	-3.1	0.005
			Co-O-Co	5.0	3.35	-4.4	0.005
Co/ ZrO_2	7709.3	7716.4	Co-O	3.9	2.04	-1.3	0.012
			Co-O-Zr	3.7	3.42	1.2	0.016

Confidence Limits for non-overlapping peaks, e.g., Co/ZrO_2: Co-O: N = ± 0.2; R = ± 0.005; σ^2 = ± 0.0005; Co-O-Zr: N = ± 0.15, R = ± 0.002; σ^2 = ± 0.0006

coprecipitation method[54] as shown in Scheme 1. For comparison, undoped ZrO_2 and Co_3O_4 impregnated ZrO_2 was synthezised via incipent wetness impregnation.

All three catalysts i.e., single atom Co/ZrO_2 catalyst, undoped ZrO_2 and Co_3O_4/ZrO_2 catalyst were characterized using powder X-ray diffraction as shown in Fig. 1. As shown in Fig. 1**A**, undoped ZrO_2 catalyst showed peaks at 30.31°, 35.29°, 50.40°, 60.36° and 63.11° corresponding to the (101), (110), (200), (211) and (202) reflections of tetragonal ZrO_2 in agreement with JCPDS# 01–080-0965.[55,56] In contrast, the cobalt doped catalyst was analysed and there was no peak corresponding to any cobalt phase, which confirms that the Co was doped into the ZrO_2 surface. The XRD pattern shows that there is shift in the (101) plane of ZrO_2 to higher 2θ value, further confirming the doping of cobalt as shown in Fig. 1**B**. This peak shift is observed due to a decrease in the interplanar spacing in ZrO_2 due to cobalt doping [57,58]. The ionic radii of Co^{+2} is 0.74 Å, less than the ionic radius of 0.84 Å for Zr^{+4} and which leads to change in lattice constant and results in shift of *t*-ZrO_2 plane to a higher 2θ value.[59] In the cobalt doped catalyst, no peak of Co_3O_4 was observed.[60] This absence of cobalt and cobalt oxide peaks in the Co/ZrO_2, supports the inference of doping of cobalt on the zirconia support. For comparison, Co_3O_4 impregnated ZrO_2 was also synthesized (**See SI**) and analysed, showing sharp peaks at 36.88°, 44.95°, 59.51° and 65.11° corresponding to the (311), (400), (511) and (440) planes of Co_3O_4 in agreement with JCPDS# 043–1003 as shown in Fig. 1**A.**[61,62] When compared with the Co/ZrO_2 catalyst, the powder XRD peak of Co_3O_4 for (311) plane was absent in case of Co/ZrO_2 suggesting the absence of nanoparticles in Co/ZrO_2 catalyst.[63] The average crystallite size was calculated using the Scherrer equation [64] and it was found to be 17 nm, 20 nm and 12 nm for Co/ZrO_2, undoped ZrO_2 and Co_3O_4/ZrO_2 respectively.

The thermal stability of Co doped ZrO_2 catalyst was analyzed by heating from 30 °C to 700 °C temperature under a nitrogen atmosphere. The thermogravimetric analysis indicates only 4% weight loss, which confirm the high thermal stability of the Co doped ZrO_2 catalyst as shown in Fig. S1. There was initial weight loss up to 200 °C due to removal of adsorbed water and further weight loss was observed due to removal of trapped organic species inside the pores of ZrO_2 support material.[51].

N_2 adsorption-desorption was performed at 1 bar pressure at 77 K temperature after degassing at 300 ℃ temperature to determine surface area, pore size and pore volume (Fig. S2). Cobalt doped ZrO_2 catalyst has a high surface area of 76 m^2/g with pore size and pore volume of 3.4 nm, and 0.061 cc/g respectively. The N_2 adsorption-desorption curve followed a type IV isotherm suggesting the formation of mesopores, which is in good agreement with the Barrett-Joyner-Halenda (BJH) pore size calculated value. Moreover, the undoped ZrO_2 and Co_3O_4 impregnated ZrO_2 was also analyzed, and all three-catalysts showed the same type of isotherm. Moreover, the calculated surface area, pore size and pore volume were found to be 69 m^2/g, 3.4 nm and 0.061 cc/g respectively for undoped ZrO_2 (see Fig. S3**(A-B)**). Additionally, the specific surface area of Co_3O_4/ZrO_2 catalyst was also calculated using the BET equation and was estimated as 46 m^2/g with a pore size and pore volume of 3.4 nm and 0.057 cc/g respectively (see Fig. S3**(C-D)**).

To confirm the atomic dispersion of cobalt atom on zirconia, aberration corrected scanning transmission electron microscopy (AC-STEM) was performed. Annular dark field (ADF) and simultaneous annular bright field (ABF) STEM images were recorded as shown in Fig. S4**.** In ABF mode, the crystalline morphology of ZrO_2 can be seen clearly as indicated by the lattice fringes **(**Fig. S4**(A-B))**. In ADF mode, there were no identifiable single Co atoms on ZrO_2 as shown in Fig. S4**(C-D)** as a result of the lower atomic number of Co relative to Zr.[65,66] It is important to note that no clusters of cobalt oxide were observed anywhere in the Co doped catalyst. Further, to confirm the dispersion of Co,

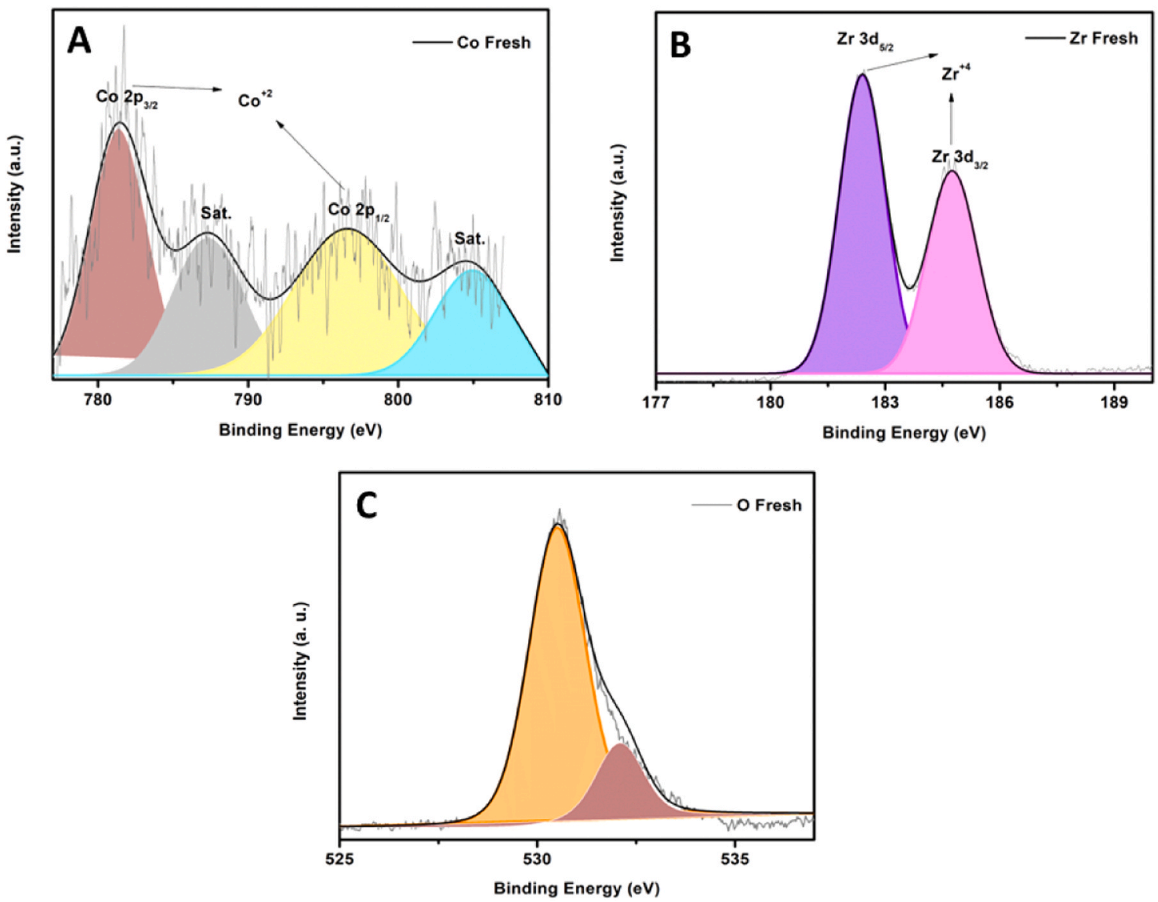

Fig. 5. XPS analysis of fresh single atom Co/ZrO_2 catalyst **(A)** Co 2p spectrum and **(B)** Zr 2p spectrum and **(C)** O 1 s spectrum.

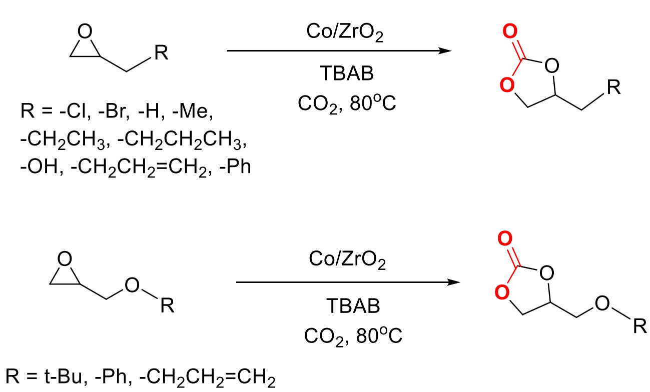

Scheme 2. General catalytic reaction of cycloaddition of CO_2 to epoxides.

Energy-dispersive X-ray spectroscopy (EDS) was performed in different regions of Co/ZrO_2 at various magnifications, as shown in Fig. S5. In each elemental map, the cobalt distribution was uniform (i.e., 6.6 ± 0.4 wt%) on ZrO_2 and no detectable Co particles on ZrO_2 were observed in the cobalt map. Similarly, the EDS results of HR-TEM and FE-SEM analysis were consistent for Co distribution on ZrO_2 as shown in Fig. 2 and Fig. S6 respectively, which suggests the atomic dispersion of cobalt on the ZrO_2 support. The lattice fringe of 0.287 nm corresponding to the (101) planes of *t*-ZrO_2 are shown in Fig. 2**B,** which is in agreement with PXRD spectra of the Co single atom catalyst (Fig. 1). The colour mapping of Co doped ZrO_2 catalyst showed uniform distribution of Co on ZrO_2 catalyst as shown in Fig. 2**C**. The SAED pattern of the Co/ZrO_2 catalyst shows the concentric rings expected from the crystalline zirconia support as shown in Fig. 2**D** inset. To confirm the content of Co and Zr metal in Co/ZrO_2 catalyst and Co_3O_4/ZrO_2 catalyst, inductively coupled plasma atomic emission spectroscopy (ICP-AES) was performed which confirmed ~6 wt% and ~9 wt% of Co content respectively (Table S1).

For comparison, STEM images of Co_3O_4 impregnated ZrO_2 were also recorded, which revealed that the catalyst has two types of morphology: one with small pores and the other with more open pore structures as shown in Fig. 3**A**. The morphology is quite distinct as seen in this figure and in some cases the two phases are joined to each other, as shown in Fig. 3**B**. The EDS analysis shows that the open pore structure comes from the Co_3O_4 phase since its concentration increases as we zoom into the open pore structure (Fig. 3**C and 3D).** The particles of Co_3O_4 can be as large as the ZrO_2 particles (Fig. S7A). However, EDS analysis shows that smaller Co_3O_4 aggregates could be dispersed on the ZrO_2 (Fig. S7C**)**. Also, in some regions of ZrO_2 there were regions suggestive of atomically dispersed Co (Fig. S7D**)**. In summary, while the cobalt doped ZrO_2 catalyst contains exclusively atomically dispersed Co, whereas in the impregnated catalyst we see phase separation of Co_3O_4 and ZrO_2. Additionally, we also see atomically dispersed Co on the ZrO_2 in the impregnated catalyst These results are in good agreement with PXRD data where the sharp (311) peak corresponding to large Co_3O_4 particles in Co_3O_4/ZrO_2 is not seen in case of the Co doped on ZrO_2.

The local Co coordination and oxidation state were analyzed via Co K-edge X-ray absorption near-edge structure (XANES) and extended X-ray absorption fine structure (EXAFS) spectroscopy, as shown in Fig. 4. The XANES energy corresponds to the dipole allowed electromagnetic transition for ionization of a 1 s electron to the 4p vacant orbitals and is taken as the first inflection point of the leading edge. For 3d compounds, the 1 s to 3d dipole forbidden transition gives a pre-edge peak. The energy of the pre-edge peak can be used to determine the oxidation

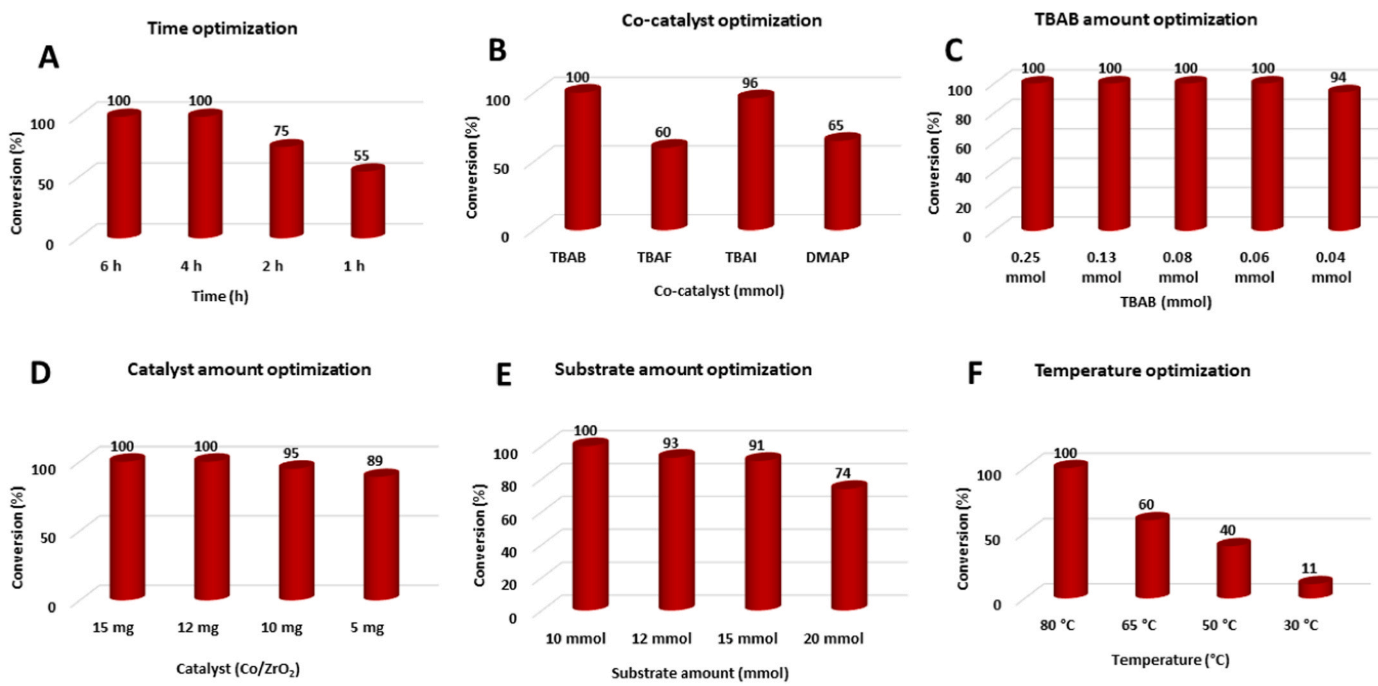

Fig. 6. Catalytic optimization of CO_2 fixation reaction at various reaction conditions. **Reaction conditions:** (**A**) substrate = 10 mmol, catalyst (Co/ZrO_2) = 15 mg, TBAB = 0.25 mmol, temperature = 80 °C, time = 1–6 h, CO_2 = 2 bar. (**B**) substrate = 10 mmol, catalyst (Co/ZrO_2) = 15 mg, TBAB = 0.25 mmol, temperature = 80 °C, time = 4 h, CO_2 = 2 bar. (**C**) substrate = 10 mmol, catalyst (Co/ZrO_2) = 15 mg, TBAB = 0.25–0.04 mmol, temperature = 80 °C, time = 4 h, CO_2 = 2 bar. (**D**) substrate = 10 mmol, catalyst (Co/ZrO_2) = 5–15 mg, TBAB = 0.06 mmol, temperature = 80 °C, time = 4 h, CO_2 = 2 bar. (**E**) substrate = 10–20 mmol, catalyst (Co/ZrO_2) = 12 mg, TBAB = 0.06 mmol, temperature = 80 °C, time = 4 h, CO_2 = 2 bar. (**F**) substrate = 10 mmol, catalyst (Co/ZrO_2) = 12 mg, TBAB = 0.06 mmol, temperature = 30–80 °C, time = 4 h, CO_2 = 2 bar.

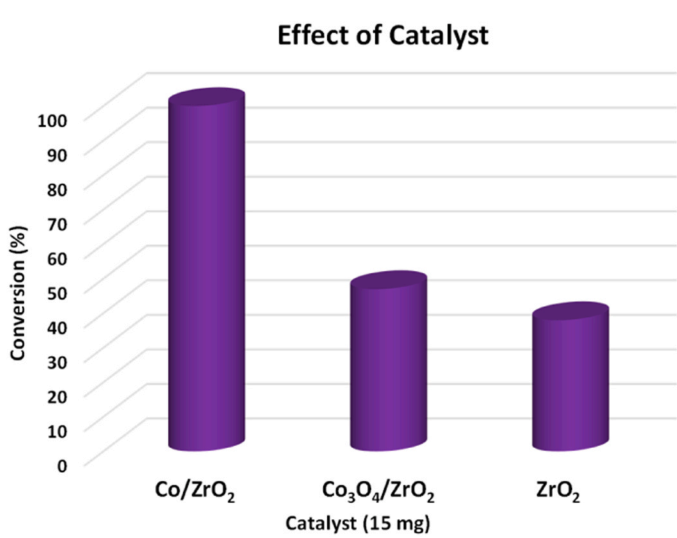

Fig. 7. Effect of different catalysts on CO_2 fixation of epichlorohydrin. **Reaction conditions:** Substrate = 10 mmol, catalyst (Co/ZrO_2) = 12 mg, CO_2 = 2 bar, TBAB = 0.06 mmol (20 mg), temp. = 80 °C, time = 4 h.

state.[67] The XANES spectra of Co foil (metallic Co) show no obvious pre-edge peak and the leading edge represents the XANES energy at 7709 eV as shown in Fig. 4**A**. The Co_3O_4/ZrO_2 reference XANES spectra shows the peak for both Co^{+2} and Co^{+3} ions. Co^{+2} is resolved in the spectrum, while Co^{+3} pre-edge peak overlaps with the Co^{+2} pre-edge peak and the leading edge of the XANES spectrum as indicated in Fig. 4**A**. For Co/ZrO_2, the pre-edge peak has the same energy as Co^{+2} with no evidence of a Co^{+3} pre-edge peak. Also, the XANES spectrum of Co/ZrO_2 is shifted to lower energy i.e. 7724 eV consistent with Co^{+2} ions present on isolated Co^{+2} on ZrO_2.[68,69] Further, Co K-edge EXAFS spectra for Co doped ZrO_2 and Co_3O_4 impregnated ZrO_2 catalyst were derived as shown in Fig. 4**B** and Fig. S8. The Fourier transform first shell fitting results of Co doped ZrO_2 and Co_3O_4/ZrO_2 catalyst along with standard Co_3O_4 and Co foil are described in Table 1.

EXAFS first-shell fitting results indicate 4 Co-O bonds at 2.03 Å of Co/ZrO_2. For comparison, there are 6 Co-O bonds at 2.13 Å in the CoO reference, while half of the Co in Co_3O_4 has 4 Co-O at 1.94 Å and 6 Co-O at 1.92 Å with higher shell Co-O-Co peaks at 2.86 and 3.31 Å. Thus, the Co-O bond distance in Co/ZrO_2 is shorter and number of bonds is smaller than those in the CoO reference. In Co/ZrO_2, there is also a very small second-shell Co-O-Zr peak at 3.42 Å indicating isolated Co^{+2} ions. Co_3O_4/ZrO_2 has 50% Co with 4 bonds and 50% Co with 6 bonds for an average Co-O coordination of 5 at 1.91 Å. In addition, there are two Co-O-Co higher shell bond distances at 2.87 Å and 3.38 Å consistent with Co_3O_4 oxide nanoparticles. The EXAFS fits are given in Table 1. These results confirmed that Co/ZrO_2 catalysts have no structure reminiscent of CoO and Co_3O_4 confirming the presence of isolated Co^{+2} in the Co doped ZrO_2 single atom catalyst. Furthermore, for comparison Co K-edge EXAFS and XANES spectra of Co_3O_4/ZrO_2 with standard Co_3O_4 was also fitted (Fig. S9 **and** Table 1) where the XANES and EXAFS of Co_3O_4 and Co_3O_4/ZrO_2 have very similar. The small differences are due to the lower Co concentration in the Co_3O_4/ZrO_2 catalyst and the strong absorption of the Co X-rays by ZrO_2. All features differ only by the weaker signal of the catalyst as shown in Table 1.

Additionally, the X-ray photoelectron spectra (XPS) of the Co/ZrO_2 catalyst were obtained. The XPS spectra of Co 2p, Zr 3d and O 1 s is shown in Fig. 5. We deconvoluted the XPS spectra (Fig. 5), where 284.8 eV was taken as reference energy. The Co 2p spectra display two peaks at 781.4 eV and 796.6 eV for Co $2p_{3/2}$ and Co $2p_{1/2}$ respectively, indicating the presence of Co^{+2} shown in Fig. 5**A**.[70–72] The Zr 3d spectra exhibited two peaks at 182.4 eV and 184.7 eV for Zr $3d_{5/2}$ and Zr $3d_{3/2}$ for tetragonal Zr^{+4} as shown in Fig. 5**B**.[25] As shown in Fig. 5**C**, O 1 s spectra exhibited two deconvoluted peaks at 530.5 eV and 532.05 eV assigned to lattice oxygen and -OH species on the surface or oxygen

Table 2
Substrate scope on CO_2 fixation of epichlorohydrin.

Entry	Substrate	Product	Time (h)	Yield[a] (%)	TOF (h^{-1})
1	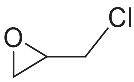	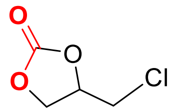	4	> 99	37.94
2	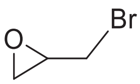	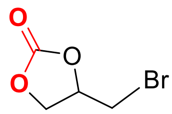	5	> 99	30.35
3	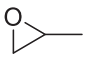	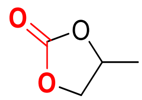	4	> 99	37.94
4	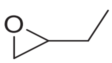	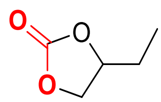	4	> 99	37.94
5	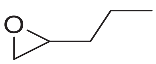	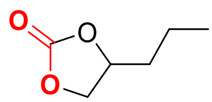	6	> 99	25.29
6	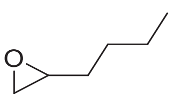	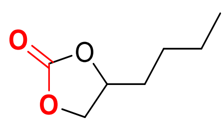	7	> 99	21.68
7	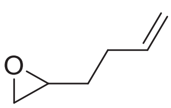	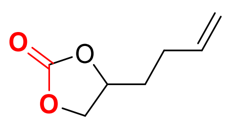	7	> 99	21.68
8	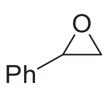	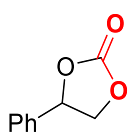	8	> 99	18.97
9	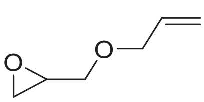	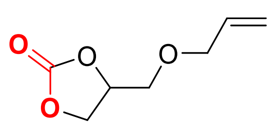	8	> 99	18.97
10	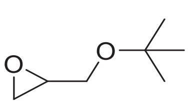	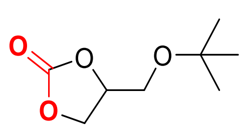	13	> 99	11.67
11	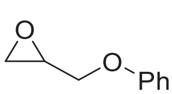	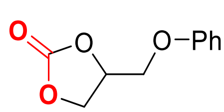	11	> 99	13.79
12	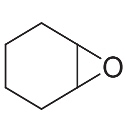	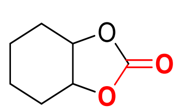	13	> 99	11.67

(continued on next page)

Table 2 (*continued*)

Entry	Substrate	Product	Time (h)	Yield[a] (%)	TOF (h^{-1})
13	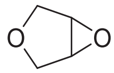	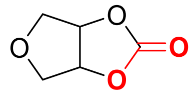	16	> 99	9.48

Reaction conditions: Substrate = 10 mmol, catalyst (Co/ZrO_2) = 12 mg, TBAB = 0.06 mmol (20 mg), temperature = 80 °C, time = 4-16 h, CO_2 = 2 bar. [a]Yield was calculated using GC-MS analysis with mesitylene as an internal standard. All the conversion and selectivity were analysed with ^1H and ^{13}C NMR.

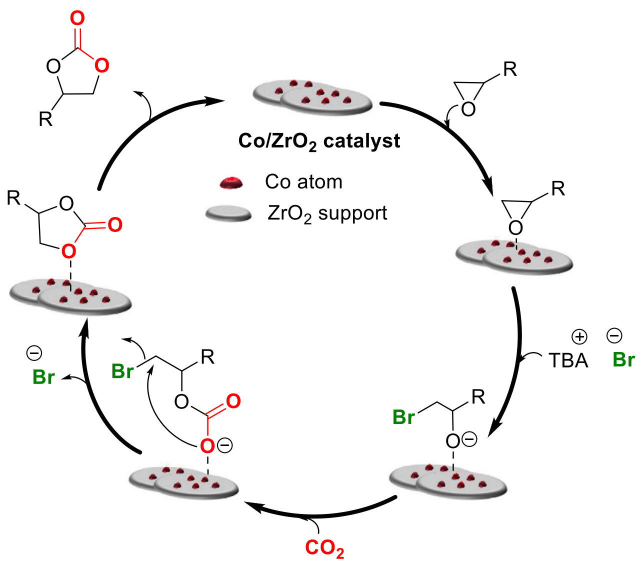

Scheme 3. A plausible mechanism of CO_2 fixation of epoxides into cyclic carbonates.

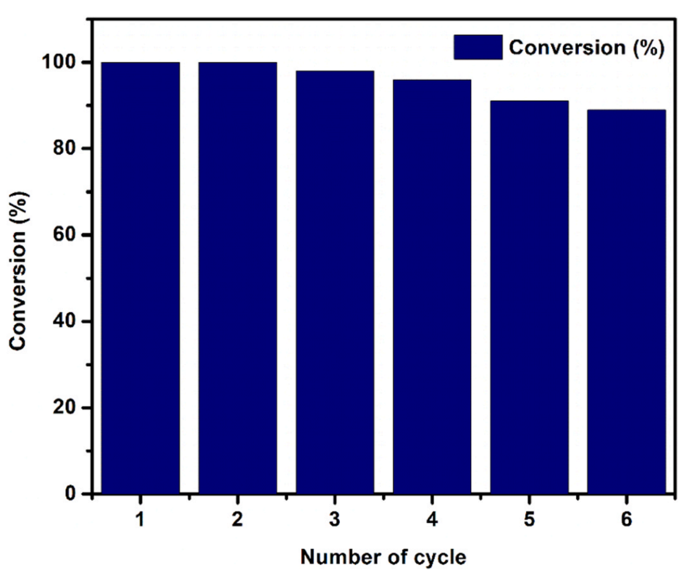

Fig. 8. Catalyst reusability of the CO_2 fixation in epichlorohydrin for all the cyclic runs. **Reaction conditions:** Substrate = 10 mmol, catalyst (Co/ZrO_2) = 12 mg, TBAB = 0.06 mmol (20 mg), temperature = 80 °C, time = 4 h, CO_2 = 2 bar.

vacancies, respectively.[73–75].

All characterization results are therefore consistent with the Co doped ZrO_2 being a single atom catalyst with uniform isolated Co^{+2} ions with no of Co_3O_4 or CoO clusters. The impregnated catalyst has a mixed structure with non-uniform dispersion of Co_3O_4 on ZrO_2.

3.2. Catalytic CO_2 fixation

The undoped ZrO_2 along with Co/ZrO_2 and Co_3O_4/ZrO_2 catalysts were tested for catalytic CO_2 fixation of epoxides to yield cyclic carbonates using tetrabutylammonium bromide (TBAB) as a co-catalyst under solvent-free conditions as shown in Scheme 2.

The reaction conditions were optimized by varying temperature, substrate, and catalyst amounts and various type of tetra butylammonium halide ion. The effect on conversion is shown in Fig. 6. For the CO_2 fixation reaction, epichlorohydrin was utilized as model substrate. Initially, the reaction was performed using 10 mmol of epichlorohydrin with 0.25 mmol of TBAB with using 15 mg of Co/ZrO_2 catalyst at 80 °C temperature for different reaction times from 1–6 h as shown in Fig. 6**A.** With decreasing the reaction time, the conversion decreases from 100 to 55%, respectively. Additional reactions were performed using different reagents i.e., tetrabutylammonium iodide (TBAI), tetrabutylammonium fluoride (TBAF), tetrabutylammonium bromide (TBAB) and 4-Dimethylaminopyridine (DMAP) for 4 h as shown in Fig. 6**B.** In absence of TBAB, there was no conversion observed indicating that TBAB is essential for the reaction and can be considered as co-catalyst for the reaction. In case of TBAB gave the highest epichlorohydrin conversion i.e., 100% into its cyclic carbonate and other reagents showed less conversion of epichlorohydrin. Hence, further optimizations were conducted using TBAB. The amount of TBAB was optimized by varying the concentration from 0.25 mmol to 0.04 mmol. At 0.04 mmol, conversion was 94% while at 0.06 mmol, the conversion was 100%, see Fig. 6**C.** Therefore, 0.06 mmol is the optimum amount for the conversion for 10 mmol of epichlorohydrin into its cyclic carbonate. Addition of DMAP gave 65% epichlorohydrin conversion, which may be due to stronger affinity of nitrogen than that of oxygen with epoxide substrate resulting in lower conversion. It appears that DMAP coordinates with catalyst's acidic sites inhibiting the adsorption of epoxide substrate.[44,76] The amount of catalyst and substrate were optimized for different reaction times as shown in Fig. 6**(D-F)**. As the catalyst amount decreases from 15 mg to 5 mg, the conversion decreases from 100% to 89%. While increasing the substrate amount from 10 mmol to 20 mmol, there is also a decrease in conversion. At room temperature, there is only 30% conversion indicating that higher reaction temperatures are required to affect epoxide, ring-opening and CO_2 fixation. The optimized reaction conditions were 10 mmol of epichlorohydrin, 12 mg of Co/ZrO_2 catalyst, 0.06 mmol of TBAB with 2 bar CO_2 at 80 °C with solvent-free reaction condition wherein 100% conversion was observed.

The effect of catalyst composition, e.g., undoped ZrO_2 and Co_3O_4 impregnated ZrO_2, was also evaluated and is shown in Fig. 7. For undoped ZrO_2, the conversion was 38%; while for Co_3O_4/ZrO_2, the conversion was 47%. The slightly higher conversion may be due to small fraction of single Co^{+2} ions. However, Co doped ZrO_2 single atom catalyst showed superior catalytic activity over both undoped ZrO_2 and Co_3O_4/ZrO_2 catalysts. These results revealed that Co doped ZrO_2 single atom catalyst provides more active sites due to presence of isolated Co^{+2} on ZrO_2 support is most suitable catalyst for cycloaddition of CO_2 to cyclic epoxides to yield cyclic carbonate with minimal amount of TBAB under solvent-free conditions.

To check the scope of the reaction, various substituted epoxides were utilized for the CO_2 fixation reaction as shown in Table 2. All substrates were converted into their corresponding cyclic carbonates at 100%

Table 3
Comparative results of some earlier reported single-atom catalysts.

S. No.	Catalyst	Substrate	TBAB	Temp (C)	Time (h)	Solvent-free	Conv (%)	Ref.
1	Zn-SAC@NC-700	Epichlorohydrin (5 mmol)	2 mol%	100	2	Yes	97	[47]
2	HPC-800 (Zn SACs)	Epibromohydrin (0.15 mmol)	0.1 mmol	300 mW/cm^2	10	No	94	[48]
3	$Au_{19}Ag_4(S\text{-}Adm)_{15}$ cluster	Epichlorohydrin (0.3 mmol)	10 mol%	60	24	No	78	[49]
4	$Au_{20}Ag_1(S\text{-}Adm)_{15}$ cluster	Epichlorohydrin (0.3 mmol)	10 mol%	60	24	No	30	[49]
5	$Au_{21}(S\text{-}Adm)_{15}$ cluster	Epichlorohydrin (0.3 mmol)	10 mol%	60	24	No	50	[49]
6	Ir/WO_3 SAC	Epichlorohydrin (1 mmol)	0.03 mmol	40	15	Yes	100	[50]
7	**Co/ZrO_2**	**Epichlorohydrin (10 mmol)**	**0.06 mmol**	**80**	**4**	**Yes**	**100**	**This work**

conversion under mild reaction conditions with minimal amount of TBAB. Both -chloro and -bromo substituted epoxides gave 100% conversion into cyclic carbonates in 4–5 h (Table 2**, Entry 1–2)**. Similarly, aliphatic substituted epoxides gave 100% conversion into their corresponding carbonates in 4–7 h (Table 2, **Entry 3–7**). However, as the aliphatic chain size increases from epoxypropane (propylene oxide) to epoxy hexane, the reaction time increases, perhaps, due to steric hindrance near the epoxide ring.[77] Finally, styrene oxide, allyl glycidyl ether, tert-Butyl glycidyl ether and phenyl glycidyl ether and other aromatic epoxides i.e. 3,6-Dioxabicyclo[3.1.0]hexane were also converted 100% into corresponding carbonates (Table 2, **Entry 8–13**). As the bulky substitute increases, the reaction time increases with decreasing catalytic activity. The effect of the bulky group was observed, in all the substrates, but complete conversions were obtained with 100% selectivity. All the conversion and selectivity were determined using ^1H and ^{13}C NMR (Fig. S10**)** and the yield was calculated through GC-MS analysis using mesitylene as an internal standard (Fig. S11).

Based on previous literature studies, the reaction mechanism of CO_2 fixation is shown in Scheme 3.[30,33,42,46,78–80] Initially, the epoxide substrate interact on the Lewis acidic Co(II) of the catalyst with oxygen atom of the epoxide and as a result of this, weakening of C-O bond of epoxide occurs. Here, in Co/ZrO_2, the single Co^{+2} ion is the active site. Subsequently, nucleophilic attack of bromide ion of TBAB occurs on the less hindered carbon atom of epoxide, which leads to ring opening of epoxy substrate.[31,45,81] Further, oxygen atom and carbon atom of CO_2 interact with positively charged cobalt and oxygen atom of epoxide, respectively. Subsequently, with removal of bromide ion cyclic carbonate formed as a product and the catalyst surface is again free for next cycle.

3.3. Recycle study and leaching test

To study the recyclability of the catalyst for CO_2 fixation of epichlorohydrin, after completion of reaction, the reactor was cooled to room temperature and reaction mixture was centrifuged and catalyst was settled down and the above solution was filtered. The filtrate was given for GC-MS analysis and the solid residue was washed with water and ethanol several times and dried overnight at room temperature. This solid residue or catalyst was then utilized for the next catalytic cycle. The catalyst was recyclable up to six cycles as shown in Fig. 8. The decrease in conversion with each regeneration is likely due to small losses in the amount of catalyst during the separation and washing of the catalyst.

Leaching tests of the catalyst were also performed using hot filtration in which the reaction was conducted for 1 h. After that, reaction mixture was filtered, and the filtrate was allowed to proceed further in presence of CO_2 without catalyst.[51,82] After completion, the conversion and selectivity were determined and confirmed that there was no significant conversion after removal of catalyst. The amount of Co in the filtrate was determined by Inductively Coupled Plasma Atomic Emission Spectroscopy (ICP-AES) and was found less than 1 ppm, Table S2**.** These studies confirm that the Co doped ZrO_2 single atom catalyst is recyclable for the cycloaddition reaction of CO_2 to epoxides.

In Table 3**,** we compare our results on CO_2 fixation of epoxides with those previously reported in the literature. Cui et al. reported zinc single atoms on N-doped carbon via simple pyrolysis of active-carbon-supported phenanthroline-ligated $Zn(OAc)_2$ complex procedure for cycloaddition of CO_2 and epoxides.[47] The reaction was performed in solvent-free conditions at comparatively high pressure and temperature i.e. 5 bar and 100°C using TBAB as additive. All the substrates (16 substrates) were converted in good to excellent yield, however only 5 mmol of substrate was utilized for the reaction (Table 3**, Entry 1)**. Yang et al. synthesized a ZIF-8 metal organic framework and derived hollow porous carbon (HPC) with uniform N-doping and loading of Zn SACs via pyrolysis.[48] The reaction was performed with epibromohydrin as substrate under light irradiation at RT, however, reaction was performed in DMF solvent and required 10 h to achieve 94% conversion (Table 3**, Entry 2)**. Li et al. synthesized $Au_{19}Ag_4(S\text{-}Adm)_{15}$ clusters, $Au_{20}Ag_1$(-S-Adm)$_{15}$ cluster and $Au_{21}(S\text{-}Adm)_{15}$ with 1-adamantanethiolate (S-Adm).[49] In $Au_{19}Ag_4(S\text{-}Adm)_{15}$, all Ag sites are open on surface, in $Au_{20}Ag_1(S\text{-}Adm)_{15}$ partially open Ag sites and in $Au_{21}(S\text{-}Adm)_{15}$ no Ag sites are present. Based on present Ag sites, their catalytic activity was in order of $Au_{19}Ag_4(S\text{-}Adm)_{15} > Au_{20}Ag_1(S\text{-}Adm)_{15} > Au_{21}(S\text{-}Adm)_{15}$. The reaction was performed with 0.3 mmol of substrates (3 substrates) using DCM/DMF solvent mixture and all three substrates showed ~80% conversion in 24 h with 10 mol% of TBAB. The reaction involved harmful solvent and involved high reaction time despite the lower amount of substrate (Table 3**, Entry 3–5)**. Xu et al. explored the strong electronic metal–support interaction in iridium single atom catalyst supported on WO_3 for CO_2 cycloaddition reaction.[50] The reaction was performed in neat condition for 1 mmol of substrate at 40 °C with 10 mg of TBAB. All substrate (6 substrates) were showed moderate to excellent yield (40–100%) in high reaction time i.e., 15 h (Table 3**, Entry 6)**.

Previous literature results utilized either low amounts of substrate with high amount of TBAB and high reaction time or utilized toxic solvents like DCM and DMF. Also, the synthesis process of previous SACs involved multistep procedures whereas our catalyst was synthesized at room temperature with using much simpler methods. Based on this, our results indicate superior catalytic performance with balanced reaction condition for chemical fixation reaction. The Co/ZrO_2 SAC is capable to convert 10 mmol of substrates with trace amount of TBAB (0.06 mmol) with 100% conversion under solvent-free conditions.

4. Conclusions

We have successfully synthesized Co doped ZrO_2 single atom catalyst via co-precipitation and characterized via STEM, XANES and EXAFS to confirm the Co is present in the form of single atoms. The EXAFS data revealed the presence of isolated Co^{+2} ions with 4 Co-O bonds at 2.04 Å. EDS elemental mapping confirmed the uniform dispersion of Co on ZrO_2 support. The as synthesized single atom catalyst was utilized for CO_2 fixation into epoxides in solvent-free condition to give high rates and selectivity of cyclic carbonates. For comparison, undoped ZrO_2 and Co_3O_4/ZrO_2 catalyst were utilized which were much less active for CO_2 fixation. These results suggest that the single atom Co^{+2} catalyst is superior to other reported single atom CO_2 fixation catalysts.

CRediT authorship contribution statement

Pham Hien: Formal analysis. **Gotluru Kedarnath:** Formal analysis. **Datye Professor Abhaya:** Formal analysis, Software, Writing – review & editing. **Miller Professor Jeffrey T.:** Formal analysis, Software, Writing – review & editing. **Tyagi Professor Avesh Kumar:** Supervision, Writing – review & editing. **Shaikh Mobin:** Conceptualization, Supervision, Writing – review & editing. **Choudhary Neha:** Conceptualization, Methodology, Writing – original draft. **jiang Shan:** Formal analysis.

Declaration of Competing Interest

The authors declare that they have no known competing financial interests or personal relationships that could have appeared to influence the work reported in this paper.

Data Availability

Data will be made available on request.

Acknowledgements

S.M.M. thanks SERB-DST, New Delhi, India (Project CRG/ 2020/ 001769), BRNS, Mumbai, India (Project 58/14/17/2020- BRNS/ 37215), and IIT Indore for financial support. N.C. thanks to UGC, New Delhi for fellowship. We are also thankful to sophisticated instrumentation centre (SIC), IIT-Indore for providing the characterization facilities. We are also thankful to 500 MHz NMR facility at the Department of Chemistry funded by DST-FIST, Government of India. We would also like to acknowledge SAIF, IIT-Bombay for HR-TEM and ICP-AES analysis and MRC at MNIT-Jaipur. Also, we would like to thank MEMS department, IIT-Indore for SEM-EDS analysis. Use of the Advanced Photon Source, an Office of Science user facility, was supported by the U.S. Department of Energy, Office of Science, Office of Basic Energy Sciences under Contract No. DE-AC02–06CH11357. The operation of the 10-BM beamline was supported by the Department of Energy and the MRCAT member institutions. Acquisition of the AC-STEM at UNM was supported by NSF DMR-1828731.

Appendix A. Supporting information

Supplementary data associated with this article can be found in the online version at doi:10.1016/j.apcatb.2023.123627.

References

[1] H. Zhang, W. Zhou, T. Chen, B.Y. Guan, Z. Li, X.W. (David) Lou, A modular strategy for decorating isolated cobalt atoms into multichannel carbon matrix for electrocatalytic oxygen reduction, Energy Environ. Sci. 11 (2018) 1980–1984, https://doi.org/10.1039/C8EE00901E.

[2] Y. Guo, S. Mei, K. Yuan, D.-J. Wang, H.-C. Liu, C.-H. Yan, Y.-W. Zhang, Low-temperature CO_2 methanation over CeO2-supported Ru single atoms, nanoclusters, and nanoparticles competitively tuned by strong metal–support interactions and H-spillover effect, ACS Catal. 8 (2018) 6203–6215, https://doi.org/10.1021/acscatal.7b04469.

[3] Y. Kwon, T.Y. Kim, G. Kwon, J. Yi, H. Lee, Selective activation of methane on single-atom catalyst of rhodium dispersed on zirconia for direct conversion, J. Am. Chem. Soc. 139 (2017) 17694–17699, https://doi.org/10.1021/jacs.7b11010.

[4] R. Qi, B. Zhu, Z. Han, Y. Gao, High-throughput screening of stable single-atom catalysts in CO_2 reduction reactions, ACS Catal. 12 (2022) 8269–8278, https://doi.org/10.1021/acscatal.2c02149.

[5] Y. Li, J. Hao, H. Song, F. Zhang, X. Bai, X. Meng, H. Zhang, S. Wang, Y. Hu, J. Ye, Selective light absorber-assisted single nickel atom catalysts for ambient sunlight-driven CO_2 methanation, Nat. Commun. 10 (2019), 2359, https://doi.org/10.1038/s41467-019-10304-y.

[6] Y. Lu, Z. Zhang, H. Wang, Y. Wang, Toward efficient single-atom catalysts for renewable fuels and chemicals production from biomass and CO_2, Appl. Catal. B: Environ. 292 (2021), 120162, https://doi.org/10.1016/j.apcatb.2021.120162.

[7] W. Zhang, W. Zheng, Single atom excels as the smallest functional material, Adv. Funct. Mater. 26 (2016) 2988–2993, https://doi.org/10.1002/adfm.201600240.

[8] J. Liu, Catalysis by supported single metal atoms, ACS Catal. 7 (2017) 34–59, https://doi.org/10.1021/acscatal.6b01534.

[9] S. Mitchell, E. Vorobyeva, J. Pérez-Ramírez, The multifaceted reactivity of single-atom heterogeneous catalysts, Angew. Chem. Int. Ed. 57 (2018) 15316–15329, https://doi.org/10.1002/anie.201806936.

[10] Y. Peng, B. Lu, S. Chen, Carbon-supported single atom catalysts for electrochemical energy conversion and storage, Adv. Mater. 30 (2018), 1801995, https://doi.org/10.1002/adma.201801995.

[11] S.C. Vasconcelos, L. Marchini, C.G.S. Lima, V.G.C. Madriaga, R.S.A. Ribeiro, V. Rossa, L.E.M. Ferreira, F. de C. da Silva, V.F. Ferreira, F.B. Passos, R.S. Varma, M.W. Paixão, T.M. Lima, Single-atom catalysts for the upgrading of biomass-derived molecules: an overview of their preparation, properties and applications, Green. Chem. 24 (2022) 2722–2751, https://doi.org/10.1039/D1GC03809E.

[12] A. Wang, J. Li, T. Zhang, Heterogeneous single-atom catalysis, Nat. Rev. Chem. 2 (2018) 65–81, https://doi.org/10.1038/s41570-018-0010-1.

[13] B. Singh, M.B. Gawande, A.D. Kute, R.S. Varma, P. Fornasiero, P. McNeice, R. V. Jagadeesh, M. Beller, R. Zbořil, Single-atom (iron-based) catalysts: synthesis and applications, Chem. Rev. 121 (2021) 13620–13697, https://doi.org/10.1021/acs.chemrev.1c00158.

[14] Q. Wu, C. Wu, Mechanism insights on single-atom catalysts for CO_2 conversion, J. Mater. Chem. A. 11 (2023) 4876–4906, https://doi.org/10.1039/D2TA06949K.

[15] S. Ji, Y. Chen, X. Wang, Z. Zhang, D. Wang, Y. Li, Chemical synthesis of single atomic site catalysts, Chem. Rev. 120 (2020) 11900–11955, https://doi.org/10.1021/acs.chemrev.9b00818.

[16] Q. Liu, Z. Zhang, Platinum single-atom catalysts: a comparative review towards effective characterization, Catal. Sci. Technol. 9 (2019) 4821–4834, https://doi.org/10.1039/C9CY01028A.

[17] L. Lin, S. Yao, R. Gao, X. Liang, Q. Yu, Y. Deng, J. Liu, M. Peng, Z. Jiang, S. Li, Y.-W. Li, X.-D. Wen, W. Zhou, D. Ma, A highly CO-tolerant atomically dispersed Pt catalyst for chemoselective hydrogenation, Nat. Nanotechnol. 14 (2019) 354–361, https://doi.org/10.1038/s41565-019-0366-5.

[18] P. Qi, J. Wang, X. Djitcheu, D. He, H. Liu, Q. Zhang, Techniques for the characterization of single atom catalysts, RSC Adv. 12 (2021) 1216–1227, https://doi.org/10.1039/D1RA07799F.

[19] L. Gong, D. Zhang, C.-Y. Lin, Y. Zhu, Y. Shen, J. Zhang, X. Han, L. Zhang, Z. Xia, Catalytic mechanisms and design principles for single-atom catalysts in highly efficient CO_2 conversion, Adv. Energy Mater. 9 (2019), 1902625, https://doi.org/10.1002/aenm.201902625.

[20] M.-M. Millet, G. Algara-Siller, S. Wrabetz, A. Mazheika, F. Girgsdies, D. Teschner, F. Seitz, A. Tarasov, S.V. Levchenko, R. Schlögl, E. Frei, Ni single atom catalysts for CO_2 activation, J. Am. Chem. Soc. 141 (2019) 2451–2461, https://doi.org/10.1021/jacs.8b11729.

[21] N. Zhang, X. Zhang, L. Tao, P. Jiang, C. Ye, R. Lin, Z. Huang, A. Li, D. Pang, H. Yan, Y. Wang, P. Xu, S. An, Q. Zhang, L. Liu, S. Du, X. Han, D. Wang, Y. Li, Silver single-atom catalyst for efficient electrochemical CO_2 reduction synthesized from thermal transformation and surface reconstruction, Angew. Chem. Int. Ed. 60 (2021) 6170–6176, https://doi.org/10.1002/anie.202014718.

[22] C. Gao, S. Chen, Y. Wang, J. Wang, X. Zheng, J. Zhu, L. Song, W. Zhang, Y. Xiong, Heterogeneous Single-Atom Catalyst for Visible-Light-Driven High-Turnover CO2 Reduction: The Role of Electron Transfer, Advanced Materials. 30 (2018) 1704624. https://doi.org/10.1002/adma.201704624.

[23] C. Zhu, S. Fu, Q. Shi, D. Du, Y. Lin, Single-atom electrocatalysts, Angew. Chem. Int. Ed. 56 (2017) 13944–13960, https://doi.org/10.1002/anie.201703864.

[24] C. Ling, Q. Li, A. Du, J. Wang, Computation-aided design of single-atom catalysts for One-Pot CO_2 capture, activation, and conversion, ACS Appl. Mater. Interfaces 10 (2018) 36866–36872, https://doi.org/10.1021/acsami.8b10394.

[25] X. Xiong, C. Mao, Z. Yang, Q. Zhang, G.I.N. Waterhouse, L. Gu, T. Zhang, Photocatalytic CO_2 reduction to CO over Ni Single atoms supported on defect-rich zirconia, Adv. Energy Mater. 10 (2020), 2002928, https://doi.org/10.1002/aenm.202002928.

[26] X. Li, A.-E. Surkus, J. Rabeah, M. Anwar, S. Dastigir, H. Junge, A. Brückner, M. Beller, Cobalt single-atom catalysts with high stability for selective dehydrogenation of formic acid, Angew. Chem. Int. Ed. 59 (2020) 15849–15854, https://doi.org/10.1002/anie.202004125.

[27] A.M. Abdel-Mageed, S. Wohlrab, Review of CO_2 reduction on supported metals (Alloys) and single-atom catalysts (SACs) for the use of green hydrogen in power-to-gas concepts, Catalysts 12 (2022) 16, https://doi.org/10.3390/catal12010016.

[28] K. Rohmann, J. Kothe, M.W. Haenel, U. Englert, M. Hölscher, W. Leitner, Hydrogenation of CO_2 to formic acid with a highly active ruthenium acriphos complex in DMSO and DMSO/Water, Angew. Chem. Int. Ed. 55 (2016) 8966–8969, https://doi.org/10.1002/anie.201603878.

[29] K. Liu, Z. Xu, H. Huang, Y. Zhang, Y. Liu, Z. Qiu, M. Tong, Z. Long, G. Chen, In situ synthesis of pyridinium-based ionic porous organic polymers with hydroxide anions and pyridinyl radicals for halogen-free catalytic fixation of atmospheric CO 2, Green. Chem. 24 (2022) 136–141, https://doi.org/10.1039/D1GC03465K.

[30] D. Prasad, K.N. Patil, J.T. Bhanushali, B.M. Nagaraja, A.H. Jadhav, Sustainable fixation of CO_2 into epoxides to form cyclic carbonates using hollow marigold CuCo2O4 spinel microspheres as a robust catalyst, Catal. Sci. Technol. 9 (2019) 4393–4412, https://doi.org/10.1039/C9CY00945K.

[31] X.-B. Lu, D.J. Darensbourg, Cobalt catalysts for the coupling of CO_2 and epoxides to provide polycarbonates and cyclic carbonates, Chem. Soc. Rev. 41 (2012) 1462–1484, https://doi.org/10.1039/C1CS15142H.

[32] A. Mitra, T. Biswas, S. Ghosh, G. Tudu, K.S. Paliwal, S. Ghosh, V. Mahalingam, Halide-free catalytic carbon dioxide fixation of epoxides to cyclic carbonates under atmospheric pressure, Sustain. Energy Fuels 6 (2022) 420–429, https://doi.org/10.1039/D1SE01513C.

[33] S.N. Ansari, P. Kumar, A.K. Gupta, P. Mathur, S.M. Mobin, Catalytic CO_2 fixation over a robust lactam-functionalized Cu(II) metal organic framework, Inorg. Chem. 58 (2019) 9723–9732, https://doi.org/10.1021/acs.inorgchem.9b00684.
[34] L.-X. You, S.-X. Yao, B.-B. Zhao, G. Xiong, I. Dragutan, V. Dragutan, X.-G. Liu, F. Ding, Y.-G. Sun, Striking dual functionality of a novel Pd@Eu-MOF nanocatalyst in C(sp 2)–C(sp 2) bond-forming and CO 2 fixation reactions, Dalton Trans. 49 (2020) 6368–6376, https://doi.org/10.1039/D0DT00770F.
[35] Y.-X. Wang, H.-M. Wang, P. Meng, D.-X. Song, J.-J. Hou, X.-M. Zhang, An uncoordinated tertiary nitrogen based tricarboxylate calcium network with Lewis acid–base dual catalytic sites for cyanosilylation of aldehydes, Dalton Trans. 50 (2021) 1740–1745, https://doi.org/10.1039/D0DT03747H.
[36] Y. Ye, B. Ge, X. Meng, Y. Liu, S. Wang, X. Song, Z. Liang, An yttrium-organic framework based on a hexagonal prism second building unit for luminescent sensing of antibiotics and highly effective CO_2 fixation, Inorg. Chem. Front. 9 (2022) 391–400, https://doi.org/10.1039/D1QI01352A.
[37] H. Chen, Z. Zhang, H. Lv, S. Liu, X. Zhang, Investigation on the catalytic behavior of a novel thulium-organic framework with a planar tetranuclear {Tm4} cluster as the active center for chemical CO_2 fixation, Dalton Trans. 51 (2022) 532–540, https://doi.org/10.1039/D1DT03646G.
[38] F.-X. Ma, F.-Q. Mi, M.-J. Sun, T. Huang, Z.-A. Wang, T. Zhang, R. Cao, A highly stable Zn9-pyrazolate metal–organic framework with metallosalen ligands as a carbon dioxide cycloaddition catalyst, Inorg. Chem. Front. 9 (2022) 1812–1818, https://doi.org/10.1039/D1QI01555A.
[39] L. Kong, Z. Li, H. Hu, J. Zhu, Z. Chen, M. Deng, Y. Ling, P. Li, Y. Jia, Y. Zhou, Reticular chemistry approach to explore the catalytic CO_2-epoxide cycloaddition reaction over tetrahedral coordination Lewis acidic sites in a Rutile-type Zinc-phosphonocarboxylate framework, Chem. Eng. J. 427 (2022), 131759, https://doi.org/10.1016/j.cej.2021.131759.
[40] M. Sinchow, N. Semakul, T. Konno, A. Rujiwatra, Lanthanide coordination polymers through design for exceptional catalytic performances in CO_2 cycloaddition reactions, ACS Sustain. Chem. Eng. 9 (2021) 8581–8591, https://doi.org/10.1021/acssuschemeng.1c01955.
[41] W. Jaroonwatana, T. Theerathanagorn, M. Theerasilp, S.D. Gobbo, D. Yiamsawas, V. D'Elia, D. Crespy, Nanoparticles of aromatic biopolymers catalyze CO 2 cycloaddition to epoxides under atmospheric conditions, Sustain. Energy Fuels 5 (2021) 5431–5444, https://doi.org/10.1039/D1SE01305J.
[42] Q.-R. Ding, Y. Yu, C. Cao, J. Zhang, L. Zhang, Stepwise assembly and reversible structural transformation of ligated titanium coated bismuth-oxo cores: shell morphology engineering for enhanced chemical fixation of CO_2, Chem. Sci. 13 (2022) 3395–3401, https://doi.org/10.1039/D1SC06847D.
[43] G. Tudu, K.S. Paliwal, S. Ghosh, T. Biswas, H.V.S.R.M. Koppisetti, A. Mitra, V. Mahalingam, para-Aminobenzoic acid-capped hematite as an efficient nanocatalyst for solvent-free CO_2 fixation under atmospheric pressure, Dalton Trans. 51 (2022) 1918–1926, https://doi.org/10.1039/D1DT03821D.
[44] A. Ghosh, G.N. Reddy, M.S.P. K, S. Chatterjee, S. Bhattacharjee, R. Maitra, S.E. Lyubimov, A.V. Arzumanyan, A. Naumkin, A. Bhaumik, B. Chowdhury, Fabrication of a hollow sphere N,S co-doped bifunctional carbon catalyst for sustainable fixation of CO2 to cyclic carbonates, Green Chem. 24 (2022) 1673–1692. https://doi.org/10.1039/D1GC04153C.
[45] Y. Sun, H. Huang, H. Vardhan, B. Aguila, C. Zhong, J.A. Perman, A.M. Al-Enizi, A. Nafady, S. Ma, Facile approach to graft ionic liquid into MOF for improving the efficiency of CO_2 chemical fixation, ACS Appl. Mater. Interfaces 10 (2018) 27124–27130, https://doi.org/10.1021/acsami.8b08914.
[46] J. Liang, Y.-Q. Xie, X.-S. Wang, Q. Wang, T.-T. Liu, Y.-B. Huang, R. Cao, An imidazolium-functionalized mesoporous cationic metal–organic framework for cooperative CO_2 fixation into cyclic carbonate, Chem. Commun. 54 (2018) 342–345, https://doi.org/10.1039/C7CC08630J.
[47] X. Cui, X. Dai, A.-E. Surkus, K. Junge, C. Kreyenschulte, G. Agostini, N. Rockstroh, M. Beller, Zinc single atoms on N-doped carbon: An efficient and stable catalyst for CO_2 fixation and conversion, Chin. J. Catal. 40 (2019) 1679–1685, https://doi.org/10.1016/S1872-2067(19)63316-4.
[48] Q. Yang, C.-C. Yang, C.-H. Lin, H.-L. Jiang, Metal–organic-framework-derived hollow N-doped porous carbon with ultrahigh concentrations of single Zn atoms for efficient carbon dioxide conversion, Angew. Chem. Int. Ed. 58 (2019) 3511–3515, https://doi.org/10.1002/anie.201813494.
[49] G. Li, X. Sui, X. Cai, W. Hu, X. Liu, M. Chen, Y. Zhu, Precisely constructed silver active sites in gold nanoclusters for chemical fixation of CO_2, Angew. Chem. 133 (2021) 10667–10670, https://doi.org/10.1002/ange.202100071.
[50] Xu, et al., Strong electronic metal–support interaction between iridium single atoms and a WO3 support promotes highly efficient and robust CO_2 cycloaddition, Adv. Mater. 34 (2022), 2206991, https://doi.org/10.1002/adma.202206991.
[51] N. Choudhary, M. Abdelgaid, G. Mpourmpakis, S.M. Mobin, CuNi bimetallic nanocatalyst enables sustainable direct carboxylation reactions, Mol. Catal. 530 (2022), 112620, https://doi.org/10.1016/j.mcat.2022.112620.
[52] T. Ressler, WinXAS: a program for X-ray absorption spectroscopy data analysis under MS-windows, J. Synchrotron Rad. 5 (1998) 118–122, https://doi.org/10.1107/S0909049597019298.
[53] J.J. Rehr, C.H. Booth, F. Bridges, S.I. Zabinsky, X-ray-absorption fine structure in embedded atoms, Phys. Rev. B. 49 (1994) 12347–12350, https://doi.org/10.1103/PhysRevB.49.12347.
[54] N.H.M. Dostagir, R. Rattanawan, M. Gao, J. Ota, J. Hasegawa, K. Asakura, A. Fukouka, A. Shrotri, Co single atoms in ZrO2 with inherent oxygen vacancies for selective hydrogenation of CO_2 to CO, ACS Catal. 11 (2021) 9450–9461, https://doi.org/10.1021/acscatal.1c02041.
[55] W.L. Vrijburg, J.W.A. van Helden, A. Parastaev, E. Groeneveld, E.A. Pidko, E.J. M. Hensen, Ceria–zirconia encapsulated Ni nanoparticles for CO_2 methanation, Catal. Sci. Technol. 9 (2019) 5001–5010, https://doi.org/10.1039/C9CY01428D.
[56] G. Ramírez-García, E.D. la Rosa, T. López-Luke, S.S. Panikar, P. Salas, Controlling trapping states on selective theranostic core@shell (NaYF 4:Yb,Tm@TiO 2 -ZrO 2) nanocomplexes for enhanced NIR-activated photodynamic therapy against breast cancer cells, Dalton Trans. 48 (2019) 9962–9973, https://doi.org/10.1039/C9DT00482C.
[57] S. Yu, H.Jin Yun, D.Minzae Lee, J. Yi, Preparation and characterization of Fe-doped TiO 2 nanoparticles as a support for a high performance CO oxidation catalyst, J. Mater. Chem. 22 (2012) 12629–12635, https://doi.org/10.1039/C2JM30360D.
[58] J. Li, B. Shen, Z. Hong, B. Lin, B. Gao, Y. Chen, A facile approach to synthesize novel oxygen-doped g -C 3 N 4 with superior visible-light photoreactivity, Chem. Commun. 48 (2012) 12017–12019, https://doi.org/10.1039/C2CC35862J.
[59] P.V. Radovanovic, D.R. Gamelin, Electronic absorption spectroscopy of cobalt ions in diluted magnetic semiconductor quantum dots: demonstration of an isocrystalline core/shell synthetic method, J. Am. Chem. Soc. 123 (2001) 12207–12214, https://doi.org/10.1021/ja0115215.
[60] C.Sheng Chua, D. Ansovini, C.J.Jun Lee, Y.Ting Teng, L.Ting Ong, D. Chi, T.S. Andy Hor, R. Raja, Y.-F. Lim, The effect of crystallinity on photocatalytic performance of Co 3 O 4 water-splitting cocatalysts, Phys. Chem. Chem. Phys. 18 (2016) 5172–5178, https://doi.org/10.1039/C5CP07589K.
[61] X. Yan, L. Tian, M. He, X. Chen, Three-dimensional crystalline/amorphous Co/Co3O4 core/shell nanosheets as efficient electrocatalysts for the hydrogen evolution reaction, Nano Lett. 15 (2015) 6015–6021, https://doi.org/10.1021/acs.nanolett.5b02205.
[62] Y.-X. Zhou, Y.-Z. Chen, L. Cao, J. Lu, H.-L. Jiang, Conversion of a metal–organic framework to N-doped porous carbon incorporating Co and CoO nanoparticles: direct oxidation of alcohols to esters, Chem. Commun. 51 (2015) 8292–8295, https://doi.org/10.1039/C5CC01588J.
[63] Y. Cao, J. Ge, M. Jiang, F. Zhang, X. Lei, Acid-etched Co3O4 nanoparticles on nickel foam: the highly reactive (311) facet and enriched defects for boosting methanol oxidation electrocatalysis, ACS Appl. Mater. Interfaces 13 (2021) 29491–29499, https://doi.org/10.1021/acsami.1c04045.
[64] N. Choudhary, T. Ghosh, S.M. Mobin, Ketone hydrogenation by using ZnO−Cu (OH)Cl/MCM-41 with a splash of water: an environmentally benign approach, Chem. – Asian J. 15 (2020) 1339–1348, https://doi.org/10.1002/asia.201901610.
[65] J. Xing, K. Takeuchi, K. Kamei, T. Nakamuro, K. Harano, E. Nakamura, Atomic-number (*Z*)-correlated atomic sizes for deciphering electron microscopic molecular images, Proc. Natl. Acad. Sci. 119 (2022), e2114432119, https://doi.org/10.1073/pnas.2114432119.
[66] S. Yamashita, J. Kikkawa, K. Yanagisawa, T. Nagai, K. Ishizuka, K. Kimoto, Atomic number dependence of Z contrast in scanning transmission electron microscopy, Sci. Rep. 8 (2018), 12325, https://doi.org/10.1038/s41598-018-30941-5.
[67] J.P. Krogman, J.R. Gallagher, G. Zhang, A.S. Hock, J.T. Miller, C.M. Thomas, Assignment of the oxidation states of Zr and Co in a highly reactive heterobimetallic Zr/Co complex using X-ray absorption spectroscopy (XANES), Dalton Trans. 43 (2014) 13852–13857, https://doi.org/10.1039/C4DT01534G.
[68] Z. Liu, Z. Xiao, G. Luo, R. Chen, C.-L. Dong, X. Chen, J. Cen, H. Yang, Y. Wang, D. Su, Y. Li, S. Wang, Defects-induced in-plane heterophase in cobalt oxide nanosheets for oxygen evolution reaction, Small 15 (2019), 1904903, https://doi.org/10.1002/smll.201904903.
[69] L. Reith, C.A. Triana, F. Pazoki, M. Amiri, M. Nyman, G.R. Patzke, Unraveling nanoscale cobalt oxide catalysts for the oxygen evolution reaction: maximum performance, minimum effort, J. Am. Chem. Soc. 143 (2021) 15022–15038, https://doi.org/10.1021/jacs.1c03375.
[70] P. Zhou, S. Zhang, Z. Ren, X. Tang, K. Zhang, R. Zhou, D. Wu, J. Liao, Y. Zhang, C. Huang, In situ cutting of ammonium perchlorate particles by co-bipy "scalpel" for high efficiency thermal decomposition, Adv. Sci. 9 (2022), 2204109, https://doi.org/10.1002/advs.202204109.
[71] S. Mia, S.J.P. Varapragasam, A. Baride, C. Balasanthiran, B. Balasubramanian, R. M. Rioux, J.D. Hoefelmeyer, Diffusion doping of cobalt in rod-shape anatase TiO 2 nanocrystals leads to antiferromagnetism, Nanoscale Adv. 2 (2020) 4853–4862, https://doi.org/10.1039/D0NA00640H.
[72] M.S. Ahmed, B. Choi, Y.-B. Kim, Development of highly active bifunctional electrocatalyst using Co3O4 on carbon nanotubes for oxygen reduction and oxygen evolution, Sci. Rep. 8 (2018), 2543, https://doi.org/10.1038/s41598-018-20974-1.
[73] A. Sinhamahapatra, J.-P. Jeon, J. Kang, B. Han, J.-S. Yu, Oxygen-deficient zirconia (ZrO2−x): a new material for solar light absorption, Sci. Rep. 6 (2016), 27218, https://doi.org/10.1038/srep27218.
[74] P. Lackner, Z. Zou, S. Mayr, U. Diebold, M. Schmid, Using photoelectron spectroscopy to observe oxygen spillover to zirconia, Phys. Chem. Chem. Phys. 21 (2019) 17613–17620, https://doi.org/10.1039/C9CP03322J.
[75] P. Lackner, J. Hulva, E.-M. Köck, W. Mayr-Schmölzer, J.I.J. Choi, S. Penner, U. Diebold, F. Mittendorfer, J. Redinger, B. Klötzer, G.S. Parkinson, M. Schmid, Water adsorption at zirconia: from the ZrO 2 (111)/Pt 3 Zr(0001) model system to powder samples, J. Mater. Chem. A 6 (2018) 17587–17601, https://doi.org/10.1039/C8TA04137G.
[76] O.P. Klenov, N.A. Chumakova, S.A. Pokrovskaya, A.S. Noskov, Modeling of heat transfer in a porous monolith catalyst with square channels, Ind. Eng. Chem. Res. 55 (2016) 3879–3889, https://doi.org/10.1021/acs.iecr.5b04804.
[77] X. Chen, M. Wei, A. Yang, F. Jiang, B. Li, O.A. Kholdeeva, L. Wu, Near-infrared photothermal catalysis for enhanced conversion of carbon dioxide under mild conditions, ACS Appl. Mater. Interfaces 14 (2022) 5194–5202, https://doi.org/10.1021/acsami.1c18889.

[78] L.-H. Liu, L. Liu, H.-R. Chi, C.-N. Li, Z.-B. Han, A [(M 2) 6 L 8] metal–organic polyhedron with high CO 2 uptake and efficient chemical conversion of CO 2 under ambient conditions, Chem. Commun. 58 (2022) 6417–6420, https://doi.org/10.1039/D2CC01734B.
[79] G. Zhai, Y. Liu, L. Lei, J. Wang, Z. Wang, Z. Zheng, P. Wang, H. Cheng, Y. Dai, B. Huang, Light-promoted CO_2 conversion from epoxides to cyclic carbonates at ambient conditions over a bi-based metal–organic framework, ACS Catal. 11 (2021) 1988–1994, https://doi.org/10.1021/acscatal.0c05145.
[80] S.-C. Ke, T.-T. Luo, G.-G. Chang, K.-X. Huang, J.-X. Li, X.-C. Ma, J. Wu, J. Chen, X.-Y. Yang, Spatially ordered arrangement of multifunctional sites at molecule level in a single catalyst for tandem synthesis of cyclic carbonates, Inorg. Chem. 59 (2020) 1736–1745, https://doi.org/10.1021/acs.inorgchem.9b02952.
[81] Y. Jung, T. Shin, K. Kim, H. Byun, S.J. Cho, H. Kim, H. Song, Rh(0)/Rh(III) core–shell nanoparticles as heterogeneous catalysts for cyclic carbonate synthesis, Chem. Commun. 53 (2016) 384–387, https://doi.org/10.1039/C6CC08318H.
[82] T. Ghosh, P. Chandra, A. Mohammad, S.M. Mobin, Benign approach for methyl-esterification of oxygenated organic compounds using TBHP as methylating and oxidizing agent, Appl. Catal. B: Environ. 226 (2018) 278–288, https://doi.org/10.1016/j.apcatb.2017.12.056.